Environ. Sci. Technol. **1999**, *33,* 1832−1839

Evidence for an Additional Oxidant in the Photoassisted Fenton Reaction

JOSEPH J. PIGNATELLO,* DI LIU,† AND PATRICK HUSTON‡

Department of Soil and Water, The Connecticut Agricultural Experiment Station, P.O. Box 1106, New Haven, Connecticut 06504-1106

The photo-Fenton reaction ($Fe^{3+} + H_2O_2 + UV$) has potential applications in wastewater treatment. This reaction was compared to H_2O_2 photolysis and other reactions that produce only hydroxyl radicals ($OH^•$) in order to probe for additional or alternative intermediates that may contribute to the recognized potency of photo-Fenton as an oxidant of organic compounds. Distinct differences were found between photo-Fenton and genuine $OH^•$ reactions. The kinetic deuterium isotope effect (KDIE) for cyclohexane in the photo-Fenton reaction increases from 1.2 to 1.4 with increasing concentration of $OH^•$ scavenger, *tert*-butyl alcohol; whereas the KDIE in genuine $OH^•$ reactions (H_2O_2/UV, Fe^{3+}/UV, and $Fe^{2+} + H_2O_2$) is 1.1 and unchanged in the presence of *tert*-butyl alcohol. Photo-Fenton catalyzed the epoxidation of cyclohexene at a much greater rate than H_2O_2/UV. The relative yields of chlorinated organic acids from 1,1,2-trichloroethane, trichloroethene, and tetrachloroethene oxidation were markedly affected by the presence of iron. Time-resolved laser flash photolysis spectroscopy in the absence of organics revealed a transient, seen only in $Fe^{3+} + H_2O_2$ solutions, with broad absorbance in the visible and a lifetime of ∼100 ns. The results suggest the participation of a high-valent oxoiron complex (ferryl) in addition to $OH^•$ in organic compound oxidations. Hydrogen peroxide forms a complex with iron, $Fe(O_2H)^{2+}$ ($K_{15} = 1.15 \times 10^{-2}$), that absorbs in the visible region and could be the precursor of the ferryl complex.

Introduction

Fenton and related reactions combine iron compounds with hydrogen peroxide or other peroxides to bring about the oxidation of organic or inorganic compounds that may be present. These reactions have broad relevance to enzymatic oxidations (*1*−*3*), synthesis (*4*), chemistry of natural waters (*5*, *6*), and treatment of hazardous wastes. Fenton-like reactions have been applied to the destruction of organic pollutants in water (e.g., refs *7*−*11*) and soil (e.g., refs *12*−*14*) under dark or light conditions. The photoassisted (photo-Fenton) reaction, which combines H_2O_2 and a ferric catalyst with light in the near-UV to visible region, is especially powerful for treating wastewater and often leads to extensive mineralization of the target pollutant (*7*−*11*). Its advantages over other advanced oxidation technologies (AOTs), such as ozonation and TiO_2 photocatalysis, have been discussed (*8, 10, 11*).

It is widely held that the active oxidant in dark and photo-Fenton systems is the hydroxyl radical ($OH^•$). The generally accepted origin of $OH^•$ in the dark is the free radical chain mechanism (*15, 16*), presented in an abbreviated form in eqs 1−4 (H_2O ligands on Fe are omitted):

$$Fe^{2+} + H_2O_2 \rightarrow Fe^{3+} + HO^- + OH^• \quad (1)$$

$$Fe^{3+} + H_2O_2 \rightarrow Fe^{2+} + HO_2^• + H^+ \quad (2)$$

$$Fe^{3+} + HO_2^• \rightarrow Fe^{2+} + O_2 + H^+ \quad (3)$$

$$OH^• + H_2O_2 \rightarrow HO_2^• + H_2O \quad (4)$$

In light, the rate of $OH^•$ formation is increased by photoreactions of H_2O_2 ($\lambda < \sim$360 nm) (*17*) and/or Fe(III) (*18*) that produce $OH^•$ directly or regenerate Fe(II) to feed into reaction 1 (eqs 5−7):

$$H_2O_2 \xrightarrow{h\nu} 2OH^• \quad (5)$$

$$Fe^{3+}(OH^-) \xrightarrow{h\nu} Fe^{2+} + OH^• \quad (6)$$

$$Fe^{3+}(L^-) \xrightarrow{h\nu} Fe^{2+} + L^• \text{ (L = organic ligand)} \quad (7)$$

In past studies of the photo-Fenton reaction (*8, 9*), we have obtained results that plausibly could be explained by the formation of an alternative oxidant in place of, or more likely in addition to, $OH^•$. The purpose of this study was to provide evidence for or against such a species.

The free radical mechanism of the Fenton reaction has been questioned from time to time, and alternatives have been proposed that involve hypothetical transients other than free $OH^•$ (*4, 16, 19*−*22*). In recent years, researchers have firmly established that complexes of iron(II) and/or iron(III) with organic ligands (e.g., porphyrin and pyridyl-type) may react with peroxides, dioxygen, or other oxidants to form a high-valent oxoiron (ferryl) moiety, Fe═O, where iron is formally in the +IV or +V oxidation state (*3, 23*−*25*). Such reactions may generate $OH^•$ concurrently, a result that has confounded the interpretation of some experiments. The ferryl moiety can oxidize organic compounds and there is general agreement that it participates in both oxygen atom and electron-transfer reactions of many heme and nonheme enzymes (*1*−*3, 23, 24*). Other forms of 'active oxygen' in reactions of hydrogen peroxide with complexed iron in organic solvents have been suggested (*4*).

In addition, it appears possible to form oxoiron(IV) or (V) species even in simple aqueous systems where only aquo ligands (H_2O, OH^-) are bound to the metal. Rush and Bielski (*26*) observed transient $H_3Fe^{V}O_4$ and its deprotonated forms upon reduction of potassium ferrate in water (pH 3.6−10) by pulse radiolysis intermediates. Ferrous ion purportedly reacts with ozone at pH 0−3 to give "FeO^{2+}" (*27*). Kremer and co-workers (*20, 28*) hypothesized the formation of "FeO^{3+}" in dark Fe(III)/H_2O_2 reactions. Shortly before our manuscript was submitted, Bossmann et al. (*29*) published evidence against $OH^•$ and in favor of an alternative oxidant, whose structure was written "Fe^{4+}_{aq}", in thermal and photo-

* Corresponding author e-mail: Joseph.Pignatello@po.state.ct.us; telephone: (203)974-8518.

† Present address: Hua Mei Electroplating Co., Ltd., 303 Bldg., San Da Electonics Zone, Zhen Xing Rd., Shen Zhen Guangdong, Peoples Republic of China 518031.

‡ Present address: Department of Chemistry, California State University, Chico, CA 95929.

10.1021/es980969b CCC: $18.00
Published on Web 04/21/1999

Fenton systems based on oxidation products of 2,4-dimethylaniline and on other arguments. Although some have offered kinetic evidence that $OH^•$ is the principal active oxidant in Fenton (*16*) or photo-Fenton (*30, 31*) systems (other than $HO_2^•$, which is largely unreactive toward organic compounds), it must be appreciated that a transient species formed together with $OH^•$ might be hard to detect if it exhibits a similar pattern of reactivity as $OH^•$ with a probe molecule, or if it reacts slower than $OH^•$ with a probe. Spin-trapping experiments are inconclusive because they do not rule out the existence of nontrapped transient or that the transient gives the same spin trap product as $OH^•$ (*32*).

Experimental Section

Reagents. The following were purchased in the highest available purity and used as received from the supplier: $NaClO_4$, $Fe(ClO_4)_2 \cdot 6H_2O$, $Fe(ClO_4)_3 \cdot xH_2O$ (0.118 g of Fe/g), cyclohexane (c-C_6H_{12}), cyclohexane-d_{12} (c-C_6D_{12}), cyclohexene (c-C_6H_{10}), cyclohexene oxide (c-$C_6H_{10}O$), dichloromethane, trichloroethene (TCE), tetrachloroethene (PCE), 1,1,2-trichloroethane (TCA), dichloroacetic acid, methyl *tert*-butyl ether, and ethylnitrosoguanidine (Aldrich Chemical Co., Milwaukee, WI); HPLC grade hexanes, *n*-decane, and ACS grade 30% hydrogen peroxide (no preservative; Fisher Scientific); *tert*-butyl alcohol (Sigma Chemical Co., St. Louis, MO); trichloroacetic acid (Brand Nu Laboratories, Meridan, CT); and dichloroacetaldehyde monohydrate (TCI American, Portland, OR). Water was purified by distillation and passage through ion-exchange and activated carbon columns (Barnstead Nanopure System) to a resistivity ≥18 MΩ-cm.

General Procedure for Photooxidation Reactions. Experiments were conducted in air-saturated aqueous solution at 0.1 M ionic strength ($NaClO_4$). Hydrogen peroxide was standardized by iodimetric titration. An Fe(III) stock solution was prepared from $Fe(ClO_4)_3$ in a small volume of acidified water ($HClO_4$). It was then diluted to the final required concentration and adjusted to pH 2.80 with $HClO_4$ or $NaHCO_3$. We followed the recommendations of Knight and Silva (*33*) to minimize oligomerization and polymerization of iron by preparing stock solutions that were dilute (≤10 mM), acidic (pH 1), and fresh. The pH was always kept below 3 regardless of $[Fe^{III}]$. In any case, solutions had no evidence of turbidity (no precipitate on a 0.2-μm filter) or absorbance above 420 nm, so it is doubtful that slight formation of colloidal oxides, if it occurred, had any effect on the analytical concentration of dissolved Fe^{III} or on the results.

Reactions were carried out in a cylindrical 380-mL borosilicate double-walled reaction vessel (hereafter, "vessel") with water circulated through the wall to maintain constant temperature of 23 or 25 °C (*9*). The vessel contained ports with PTFE-lined screw caps for sampling and introduction of reagents. The photochemical reactor chamber (Rayonet RPR-200) was equipped with 16 14-W fluorescent black lamps supplied with the instrument that emits in the range 300−400 nm with maximum intensity about 360 nm. The lamps were warmed for at least 10 min prior to reaction to obtain constant output. The intensity in the vessel was 1×10^{19} quanta $s^{-1}\,L^{-1}$ as measured by ferrioxalate actinometry. The vessel was filled with a solution containing iron and the organic compounds to leave minimal headspace. Reaction was initiated by injecting H_2O_2 stock solution through a septum, quickly inserting the vessel into the chamber with the warmed lamps momentarily turned off, and restarting the lamps. The solution was stirred by a magnetic stir bar. Samples were withdrawn at timed intervals by syringe via Teflon tubing fitted through the septum and immediately extracted into dichloromethane or hexane for GC analysis. Dark experiments were carried out in PTFE-lined screw cap 250-mL Erlenmeyer flasks at ambient temperature in a room illuminated with dim red light.

Complexation of Fe^{3+} with H_2O_2. Absorption spectra were taken on a Hewlett-Packard 8452 diode array spectrophotometer. Solutions of 0.2 mM Fe^{3+} and 0−900 mM H_2O_2 were mixed in 0.1 M $NaClO_4$ at pH 2.80 or pH 1.45, and the spectrum was recorded immediately. The solution was then immediately titrated for H_2O_2 in the presence of 0.12 M NH_4F added to prevent interference from Fe(III) (*7*). Spectra were stable, and no significant loss of H_2O_2 titer took place over at least 0.5 h. For purposes of calculation, spectra were background-subtracted for H_2O_2.

Competition Kinetics: Theory. Competition kinetics are used to compare the reactivities of solutes present together in the same solution and, thus, under absolutely identical conditions. For A and B undergoing rate-limiting elementary bimolecular reactions with a common reactant, e.g., $OH^•$ (eq 8) in the same homogeneous reaction solution, the integrated rate laws are in eq 9:

$$\mathrm{A(B)} + \mathrm{OH}^\bullet \xrightarrow{k^{\mathrm{OH}}_{\mathrm{A(B)}}} \text{products of A(B)} \qquad (8ab)$$

$$-\ln\frac{[\mathrm{A}]_t}{[\mathrm{A}]_0} = k^{\mathrm{OH}}_{\mathrm{A}}\int_0^t[\mathrm{OH}]\,\mathrm{d}t\,;\; -\ln\frac{[\mathrm{B}]_t}{[\mathrm{B}]_0} = k^{\mathrm{OH}}_{\mathrm{B}}\int_0^t[\mathrm{OH}]\,\mathrm{d}t \qquad (9ab)$$

Since the yield of $OH^•$ is identical, eqs 9a and 9b can be combined to give eq 10. Thus, the slope of the ln−ln plot of the concentrations of A and B as they change over time affords k^{OH}_A/k^{OH}_B:

$$\ln\frac{[\mathrm{A}]_t}{[\mathrm{A}]_0} = \frac{k^{\mathrm{OH}}_{\mathrm{A}}}{k^{\mathrm{OH}}_{\mathrm{B}}}\ln\frac{[\mathrm{B}]_t}{[\mathrm{B}]_0} \qquad (10)$$

Participation of a second oxidant (ox) as in eq 11 gives overall integrated rate laws for A and B expressed in eq 12.

$$\mathrm{A(B)} + \mathrm{ox} \xrightarrow{k^{\mathrm{ox}}_{\mathrm{A(B)}}} \text{products of A(B)} \qquad (11ab)$$

$$\ln\frac{[\mathrm{A}]_t}{[\mathrm{A}]_0} = \int_0^t(k^{\mathrm{OH}}_{\mathrm{A}}[\mathrm{OH}] + k^{\mathrm{ox}}_{\mathrm{A}}[\mathrm{ox}])\,\mathrm{d}t\,;\; -\ln\frac{[\mathrm{B}]_t}{[\mathrm{B}]_0} = \int_0^t(k^{\mathrm{OH}}_{\mathrm{B}}[\mathrm{OH}] + k^{\mathrm{ox}}_{\mathrm{B}}[\mathrm{ox}])\,\mathrm{d}t \qquad (12ab)$$

Taking their ratio results in eq 13:

$$\ln\frac{[\mathrm{A}]_t}{[\mathrm{A}]_0} = \left\{\frac{k^{\mathrm{OH}}_{\mathrm{A}}\int_0^t[\mathrm{OH}]\,\mathrm{d}t + k^{\mathrm{ox}}_{\mathrm{A}}\int_0^t[\mathrm{ox}]\,\mathrm{d}t}{k^{\mathrm{OH}}_{\mathrm{B}}\int_0^t[\mathrm{OH}]\,\mathrm{d}t + k^{\mathrm{ox}}_{\mathrm{B}}\int_0^t[\mathrm{ox}]\,\mathrm{d}t}\right\}\ln\frac{[\mathrm{B}]_t}{[\mathrm{B}]_0} \qquad (13)$$

In this case, the slope of a ln−ln plot of normalized concentrations of the competing solutes will be equal to the term in large braces in eq 13. The deviation of the slope of eq 10 from that of eq 13 depends on the yields of ox and $OH^•$ integrated over time and the values of $k^{OH}_{A(B)}$ and $k^{ox}_{A(B)}$.

Cyclohexane Kinetic Deuterium Isotope Effect (KDIE) Determined by Competition Kinetics. A solution containing equal concentrations of c-C_6H_{12} and c-C_6D_{12} was placed in the reaction vessel, allowing only 1−2 cm^3 headspace to minimize volatization, and reacted as described in the general procedure. Dichloromethane extracts of samples taken at intervals were analyzed by GC/FID on a DB-624 column (38 °C for 0.5 min followed by 0.5 °C/min ramp to 41 °C, then by a 65 °C/min ramp to 165 °C, and finally held at 165 °C for 3 min) with *n*-decane as an internal standard. The ratio of rate constants (KDIE) was obtained from data up to ~75−90% loss of starting materials as the slope of eq 10 or eq 13, whichever is appropriate.

Oxidation of Cyclohexene. Reactions were performed using a two-phase mixture of aqueous reagent solution and c-C_6H_{10} (100 mL each) with vigorous stirring. The reaction

vessel in this case was a 250-mL PTFE-lined screw cap Erlenmeyer flask illuminated (or not) by a black lamp. We did not measure photon intensity in this apparatus. Samples of the organic phase were analyzed by GC on the DB-624 column (53 °C for 3 min followed by 10 °C/min ramp to 75 °C and held for 10 min at 75 °C) and products were identified by GC/MS.

Products of Chlorinated Hydrocarbons. Chlorinated degradation products of TCA, PCE, and TCE were determined in single-solute experiments. Samples withdrawn (5 mL) were acidified with 0.15 mL of 50% H_2SO_4 and frozen in dry ice. These samples were later thawed and extracted twice with 4−5 mL of methyl *tert*-butyl ether. Derivatization of the carboxylic acids present was carried out with diazoethane, prepared from ethylnitrosoguanidine in a manner analogous to the customary preparation of diazomethane (*34*). *Caution: Diazoethane, which may be carcinogenic and explosive, should be handled in an efficient hood and behind a safety shield*. These samples were analyzed by GC/ECD on the DB-624 column: 40 °C for 7 min followed by 3 °C/min ramp to 100 °C. Products were confirmed by GC/MS (HP5890 GC interfaced to HP 5988A quadrapole MS) in comparison with prepared standards.

Time-Resolved Fast Kinetics. Nanosecond laser flash photolysis experiments were carried out at the DOE Radiation Laboratory, University of Notre Dame. Samples were placed in a 6 mm × 10 mm rectangular quartz cell. Laser pulses (∼6 ns pulse width; 4−5 mJ/pulse) provided by a Quanta Ray Model DCR-1 Nd:YAG System, using a 355 nm (third harmonic) for excitation, were passed through the 6-mm face of the cell. The laser output was attenuated and defocused to minimize multiphotonic processes. Probe light provided by a Xe lamp was passed perpendicular to the pulse light. The photomultiplier output was digitized with a Tektronix 7912 AD programmable digitizer. The experiments were controlled by an LSI-11 microprocessor interfaced to a Microvax 3400 computer. The signal represents the absorbance of photoinduced intermediates with reactants as reference. Data were averaged over five replicate pulses.

Results and Discussion

Speciation of Fe(III) in Acidic Dilute Hydrogen Peroxide Solutions. It may be hypothesized that an alternative oxidant arises from a precursor iron(III) peroxo complex. Such complexes are proposed intermediates in the catalytic decomposition of hydrogen peroxide (*15*, *16*, *20*, *35*). Ferric ion undergoes hydrolysis in water to give $Fe(OH)^{2+}$, $Fe(OH)_2^{+}$, $Fe_2(OH)_2^{4+}$, $Fe(OH)_3^{0}$, and higher oligomers and insoluble polymers of iron oxide (*33*). Below pH ∼3, hexaaquo and hydroxopentaaquo ions predominate (eq 14; coordinated H_2O omitted):

$$Fe^{3+} + H_2O \rightleftharpoons Fe(OH)^{2+} + H^+;\ K_{14} = \frac{[Fe(OH)^{2+}][H^+]}{[Fe^{3+}]} \qquad (14)$$

with $K_{14} = 2.89 \times 10^{-3}$ M ($\mu = 0.1$ M; *35*). At pH 2.8, the ratio $[Fe(OH)^{2+}]/[Fe^{3+}]$ is 1.8.

Complexation between H_2O_2 and Fe^{3+} has been observed in solutions of high $[H_2O_2]$ (up to ∼0.75 mole fraction) by spectroscopic changes in the visible region (*36*, *37*). Evans et al. (*37*) observed reaction 15 [$K_{15} = 3.65\ (\pm 0.7) \times 10^{-3}$]. Lewis et al. (*36*) confirmed reaction 15 [$K_{15} = 1.98 \times 10^{-3}$] and found evidence at very high $[H_2O_2]$ for $Fe(H_2O_2)^{3+}$ [eq 16, $K_{16} = 3.2 \times 10^{-2}\ M^{-1}$] and $Fe(H_2O_2)(O_2H)^{2+}$ [eq 17, $K_{17} = \sim 6.6 \times 10^{-4}$]. In dilute H_2O_2 solution typical of our conditions, the predominant iron(III) peroxo complex is predicted to be $Fe(O_2H)^{2+}$, while the others involving neutral H_2O_2 ligands should exist only at trace levels.

$$Fe^{3+} + H_2O_2 \rightleftharpoons Fe(O_2H)^{2+} + H^+ \qquad (15)$$

$$Fe^{3+} + H_2O_2 \rightleftharpoons Fe(H_2O_2)^{3+} \qquad (16)$$

$$Fe(H_2O_2)^{3+} + H_2O_2 \rightleftharpoons Fe(H_2O_2)(O_2H)^{2+} + H^+ \qquad (17)$$

Addition of H_2O_2 to 2×10^{-4} M Fe^{III} at pH 2.8 in the dark results in an immediate change from the yellow-orange color of $Fe(OH)^{2+}$ to a brownish color. The spectrum (Figure 1) shows the growth of absorbance at 380−650 nm as $[H_2O_2]$ increases from 0 to 0.9 M. Supporting the equilibrium in eq 15, (a) the signal is suppressed at pH 1.45 and (b) a drop in pH is observable at higher H_2O_2 (∼2 M). Combining the equilibrium expressions for reactions 14 and 15 with the mass balance law, $[Fe^{III}] = [Fe^{3+}] + [Fe(OH)^{2+}] + [Fe(O_2H)^{2+}]$, and assuming Beer's law leads to eq 18, where A_{450} is the solution absorbance at 450 nm (where Fe^{3+} and $Fe(OH)^{2+}$ are transparent), l is the path length (cm), and ϵ_{FeP} ($M^{-1}\ cm^{-1}$) is the molar extinction coefficient of $Fe(O_2H)^{2+}$:

$$\frac{1}{A_{450}} = \frac{[H^+] + K_{14}}{[Fe^{III}] l \epsilon_{FeP} K_{15}} \cdot \frac{1}{[H_2O_2]} + \frac{1}{[Fe^{III}] l \epsilon_{FeP}} \qquad (18)$$

Plots of A_{450}^{-1} vs $[H_2O_2]^{-1}$ are linear (Figure 1, inset). The values of ϵ_{FeP} and K_{15} may be obtained from the intercept and slope of eq 18. At pH 2.8, $\epsilon_{FeP} = 420(\pm 65)\ M^{-1}\ cm^{-1}$ and $K_{15} = 9.0\ (\pm 1.5) \times 10^{-3}$; similarly, at pH 1.45, $\epsilon_{FeP} = 400 \pm 130\ M^{-1}\ cm^{-1}$ and $K_{15} = 14\ (\pm 5) \times 10^{-3}$. The average ϵ_{FeP} at 450 nm ($423\ M^{-1}\ cm^{-1}$) agrees with the literature (∼$446\ M^{-1}\ cm^{-1}$; *37*). The average K_{15} (1.15×10^{-2}) is 3−5 times larger than reported values (*36*, *37*); however, the extremely high $[H_2O_2]$ used in those studies may have affected bulk solvent properties.

The fraction of Fe^{III} present as $Fe(O_2H)^{2+}$ is given by the following: $[Fe(O_2H)^{2+}]/[Fe^{III}]_T = K_{15}[H_2O_2]/(K_{14} + [H^+] + K_{15}[H_2O_2])$; thus, for example, at optimal photo-Fenton pH (2.8), at typical $[H_2O_2]$ employed for contaminant degradation (∼0.01−0.1 M) (*8*, *9*; this study), and using the average K_{15}, the complex $Fe(O_2H)^{2+}$ comprises 2.5−20% of total Fe^{III}. We conclude that $Fe(O_2H)^{2+}$ may comprise a significant fraction of total Fe^{III}, even at modest peroxide levels.

Kinetic Deuterium Isotope Effect (k_H/k_D) for Cyclohexane. The KDIE for cyclohexane was measured by following the rates of loss of *c*-C_6H_{12} and *c*-C_6D_{12} using the same-pot competition kinetic method. Equations 19 and 20 are relevant.

$$c\text{-}C_6H_{12}(D_{12}) + OH^{\bullet} \xrightarrow{k^{OH}_{H(D)}} \text{product} \qquad (19)$$

$$c\text{-}C_6H_{12}(D_{12}) + \text{ox} \xrightarrow{k^{ox}_{H(D)}} \text{product} \qquad (20)$$

If reaction 19 is the only decomposition pathway, the appropriate rate law is eq 10 above, where A and B are *c*-C_6H_{12} and *c*-C_6D_{12} and the slope k_A^{OH}/k_B^{OH} represents the KDIE. If reaction 20 also occurs, the KDIE will be defined by the term in large braces in eq 13.

The results are given in Table 1, and Figure 2 shows a typical plot represented by the H_2O_2/UV (no iron) reaction. The cyclohexane KDIE in the H_2O_2/UV reaction or in the Fe^{3+}/UV reaction (no H_2O_2; eq 6), where $OH^{\bullet}$ is the only plausible oxidant, ranges from 1.07 to 1.12, with standard errors of ≤3%. Likewise, the cyclohexane KDIE for the classical Fenton reaction ($Fe^{2+} + H_2O_2$ in the dark; eq 1) is 1.06 ± 0.08, close to a reported value of 1.0−1.1 for the same reaction (*38*) and consistent with the widely held assumption that $OH^{\bullet}$ is its sole product.

On the other hand, the KDIE was significantly greater in the photo-Fenton system, which gave values in separate determinations of 1.22 and 1.26 (± ≤4%). The difference in

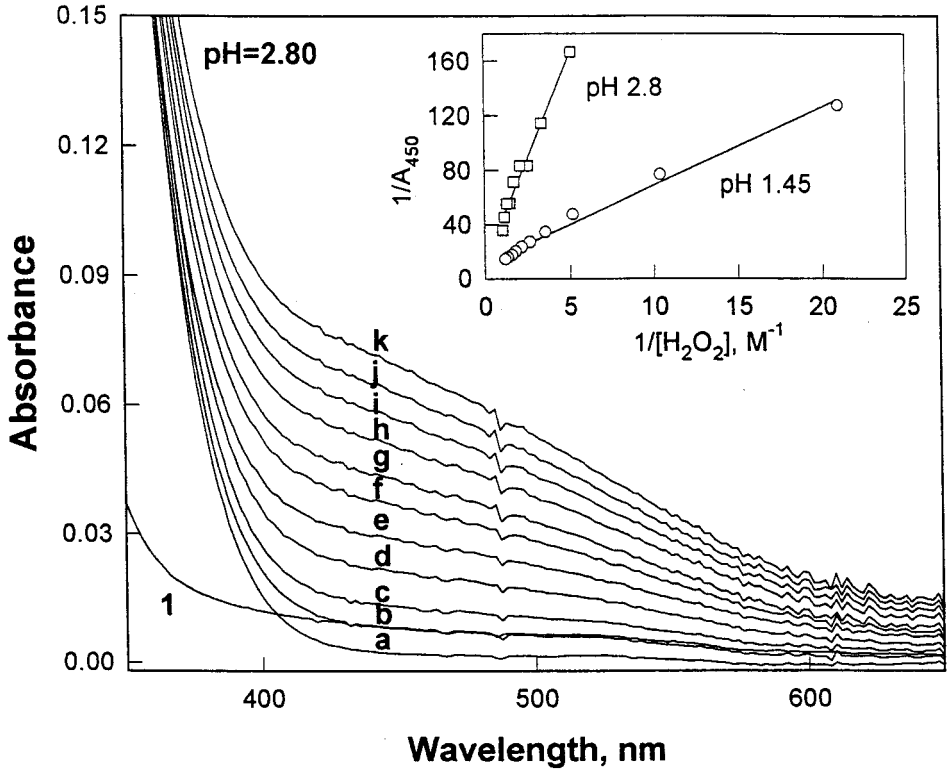

FIGURE 1. Absorption spectra of 0.2 mM Fe^{3+} with incremental H_2O_2 addition at pH 2.80 ± 0.01, μ = 0.1 M. Concentration of H_2O_2 was (a) 0, (b) 50, (c) 100, (d) 200, (e) 300, (f) 400, (g) 500, (h) 600, (i) 700, (j) 800, and (k) 900 mM. Spectrum 1 is 900 mM H_2O_2 only. Inset shows the double-reciprocal plots of A_{obs} at 450 nm and $[H_2O_2]$ according to eq 18 at pH 2.8 and pH 1.45. The slope and interception yield K_{15} and ϵ_{FeP} for the complex $Fe(O_2H)^{2+}$.

TABLE 1. Cyclohexane Kinetic Deuterium Isotope Effect under Various Conditions

reaction	conditions[a]	k_H/k_D[b]
H_2O_2/UV	0.6 M H_2O_2	1.08 ± 0.02; 1.12 ± 0.01
Fe^{3+}/UV	1 mM Fe^{3+}	1.12 ± 0.02
classic Fenton (Fe^{2+}/H_2O_2)[c]	1 mM Fe^{2+} and 10 mM H_2O_2	1.06 ± 0.08
photo-Fenton (Fe^{3+}/H_2O_2/UV)	1 mM Fe^{3+} and 10 mM H_2O_2	1.26 ± 0.05; 1.22 ± 0.03

[a] Ionic strength = 0.1 M ($NaClO_4$), pH 2.8 ± 0.01. [b] ± standard error of slope of eqs 10 or 13. [c] Fe^{2+} added dropwise to a solution of H_2O_2 and cyclohexane in water.

KDIE between the photo-Fenton and the OH•-only systems, while small, is statistically significant. This suggests an additional pathway for cyclohexane loss in the photo-Fenton reaction since otherwise the KDIE should be identical.

The second oxidant appears to have a cyclohexane KDIE of around 1.4. This was determined by adding incremental amounts of *tert*-butyl alcohol. *tert*-Butyl alcohol is an efficient scavenger of OH• (k^{OH}_{t-but} = 6.0 × 10^8 M^{-1} s^{-1}) (*38*) but is believed to be less reactive toward high valent oxoiron complexes (*25*). Figure 3A shows that the H_2O_2/UV reaction with cylcohexane is more strongly inhibited by *tert*-butyl alcohol than is the photo-Fenton reaction. The psuedo-first-order k_H of H_2O_2/UV reaction approaches zero at high [*tert*-butyl alcohol], while that of photo-Fenton approaches a nonzero value at high [*tert*-butyl alcohol]. Figure 3B shows that the KDIE of cyclohexane under photo-Fenton conditions increases smoothly from 1.2 in the absence of *tert*-butyl alcohol to 1.4 in the presence of 3 × 10^{-2} M or greater *tert*-butyl alcohol. These results imply that the photo-Fenton reaction generates a mixture of OH• and another reactive oxidant, the former suppressed by *tert*-butyl alcohol. Figure 3B also shows that the cyclohexane KDIE for H_2O_2/UV is

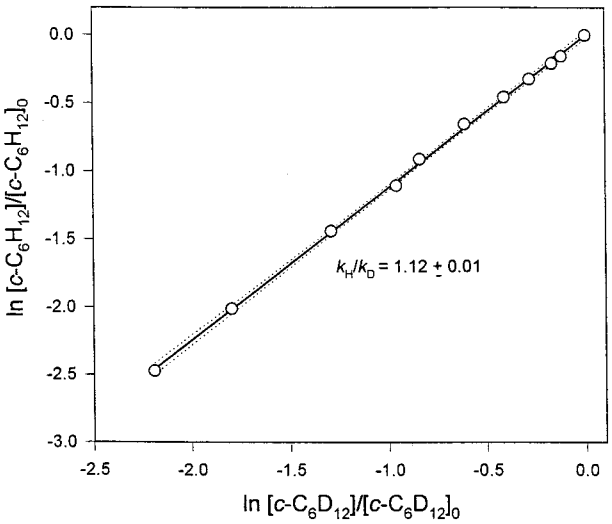

FIGURE 2. Competitive kinetic plot cyclohexane and cyclohexane-d_{12} in the H_2O_2/UV reaction; 0.6 M H_2O_2, 0.2 mM $C_6H(D)_{12}$ at pH 2.79−2.81 and ionic strength = 0.1 M. The slope yields the kinetic deuterium isotope effect for reaction of •OH with cyclohexane. The dotted curves represent the 99% confidence intervals.

independent of [*tert*-butyl alcohol] up to at least 7 × 10^{-2} M. This rules out the possibility that the KDIE of 1.4 in photo-Fenton at high [*tert*-butyl alcohol] is due to H abstraction by peroxyl or alkoxyl radicals, since those radicals should predominate also under conditions of high [*tert*-butyl alcohol] in the H_2O_2/UV reaction. As will be discussed later, a KDIE of 1.4 is consistent with reported KDIE of some chelated high-valent oxoiron complexes.

Epoxidation of Cyclohexene. Alkene epoxidation is uncharacteristic of OH• but well-known for ferryl complexes

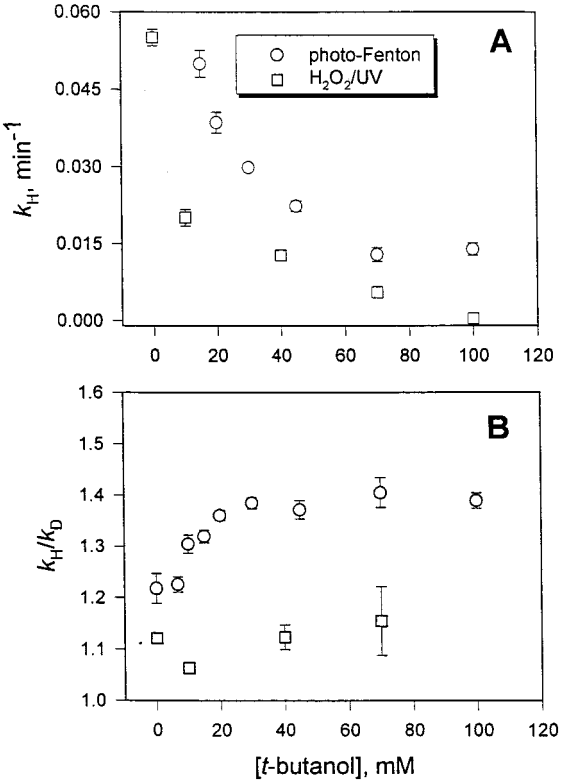

FIGURE 3. Cyclohexane oxidation as affected by addition of *tert*-butyl alcohol as scavenger in peroxide photolysis as compared with photo-Fenton reactions. Conditions: H_2O_2/UV, $[H_2O_2] = 0.6$ M; $Fe^{3+}/H_2O_2/h\nu$, $[Fe^{3+}] = 1$ mM, $[H_2O_2] = 10$ mM; both, *c*-$C_6H(D)_{12}$ = 0.2 mM, pH 2.8, ionic strength = 0.1 M. (Panel A) Dependence of the *c*-C_6H_{12} rate constant on [*tert*-butyl alcohol]. (Panel B) Kinetic deuterium isotope effect as a function of [*tert*-butyl alcohol]. The error bar, which is smaller than the symbol in some cases, represents the standard error of slope of the first-order kinetic plot.

(e.g., refs *39* and *40*). The possibility that epoxidation was taking place in photo-Fenton reactions was probed with *c*-C_6H_{10}, and the results are shown in Figure 4. To minimize hydrolysis of the expected product, cyclohexene oxide (*c*-$C_6H_{10}O$), under the acidic conditions of the aqueous phase, the reaction was carried out in a well-agitated two-phase mixture containing neat *c*-C_6H_{10} and the aqueous reactants in order to continuously extract *c*-$C_6H_{10}O$ into the organic phase as it formed. This also provided a constant concentration of *c*-C_6H_{10} in the aqueous phase (solubility, ~0.7 mM). The oxidation reactions occur only in the aqueous phase due to the insolubility of the inorganic reactants in the organic phase and the extremely short lifetime of the oxidants, which precludes their transport into the organic phase. In preliminary homogeneous experiments (data not shown), the concentrations of Fe and H_2O_2 of the photo-Fenton and H_2O_2 in the H_2O_2/UV reactions were adjusted to equalize the rates of *c*-C_6H_{10} loss so that the epoxide yield in the two-phase experiments could be directly compared. These concentrations are specified in the legend to Figure 4. In addition to photo-Fenton and H_2O_2/UV reactions, we carried out controls under otherwise identical conditions in which we reacted (A) cyclohexene with H_2O_2 in the dark (no Fe) and (B) cyclohexene under UV irradiation (no H_2O_2, no Fe). With these controls, we could establish the influence of iron and rule out contributions of side reactions such as photolysis of cyclohexene or its intermediates.

The total ion chromatograms of the cyclohexene phase obtained after 60 min reaction under the two-phase conditions (Figure 4A) were almost identical for the photo-Fenton and H_2O_2/UV reactions except for peaks A and F. Peak A,

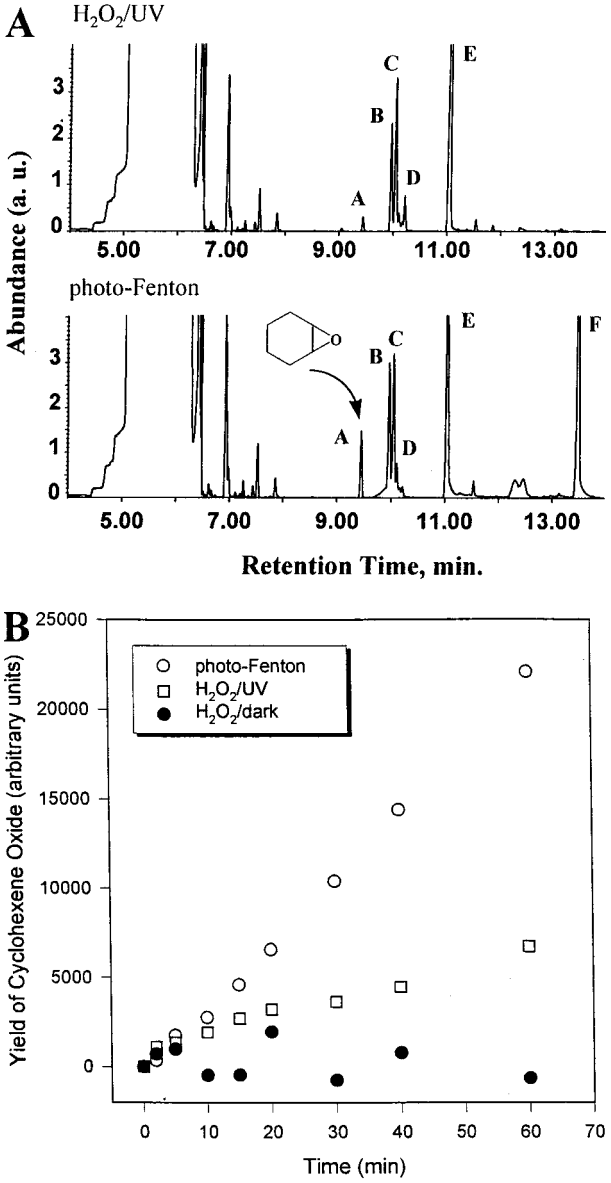

FIGURE 4. Oxidation of cyclohexene by the photo-Fenton reaction as compared with hydrogen peroxide photolysis. Conditions were adjusted to equalize the rates of loss of cyclohexene ($C_0 = 0.6$ mM): H_2O_2/UV, $[H_2O_2] = 0.6$ M, pH 2.00; Fe^{3+}/H_2O_2/UV, $[Fe^{3+}] = 0.2$ mM, $[H_2O_2] = 2$ mM, pH 2.00. Then, reactions were carried out in a two-phase mixture (*c*-C_6H_{10}/H_2O) to continually extract products. (Panel A) Total ion chromatogram of *c*-C_6H_{10} layer. Peaks: A, 7-oxabicyclo[4.1.0]heptane (cyclohexene oxide); B, cyclohexanol; C, 2-cyclohexen-1-ol; D, cyclohexanone; E, 2-cyclohexan-1-one; F, unidentified. (Panel B) Yield of cyclohexene oxide with time.

identified as *c*-$C_6H_{10}O$ by comparison with a standard, is much more intense in the photo-Fenton reaction. Peak F has not yet been identified, but it is only produced in the photo-Fenton reaction. The other peaks identified on the basis of library matching were cyclohexanol, 2-cyclohexen-1-ol, cyclohexanone, and 2-cyclohexen-1-one; these products could originate from $OH^\bullet$ or other oxidants. Figure 4B shows that the growth of the epoxide, peak A, is 3−4 times faster in the photo-Fenton reaction than in the H_2O_2/UV reaction. The cyclohexene oxide in the H_2O_2/UV reaction is due possibly to its epoxidation by acyl radicals, $RCO_2^\bullet$ (*41*, *42*). No epoxide was formed in dark reactions and in the absence of iron, showing that H_2O_2 itself is unreactive with respect to *c*-C_6H_{10} epoxidation. Also, no epoxide was formed when cyclohexene alone was photolyzed.

TABLE 2. Product Yields as Percent of Reacted Starting Material of 1,1,2-Trichloroethane, Trichloroethene, and Tetrachloroethene Comparing Photo-Fenton and H_2O_2/UV Reactions

reactant	product	% yield in photo-Fenton reaction[a]	% yield in H_2O_2/UV reaction[b]
Cl_2CHCH_2Cl	Cl_2CHCHO	4.4	2.0
Cl_2CHCH_2Cl	Cl_2CHCO_2H	5.2	0.5
Cl_2CHCH_2Cl	$ClCH_2CO_2H$	16.0	47
$Cl_2C{=}CCl_2$	Cl_3CCO_2H	3.7	0.11
$Cl_2C{=}CCl_2$	Cl_2CHCO_2H	0.2	0.18
$Cl_2C{=}CHCl$	Cl_3CCO_2H	trace[c]	trace[c]
$Cl_2C{=}CHCl$	Cl_2CHCO_2H	2.7	0.12
$Cl_2C{=}CHCl$	Cl_2CHCHO	nd[d]	nd

[a] Conditions: 5.6×10^{-6} M Fe(III), 1.0×10^{-3} M H_2O_2, pH 2.80 ± 0.02, 25.0 °C. [b] Conditions: 5.0×10^{-2} M H_2O_2, pH 2.80 ± 0.02, 25.0 °C. [c] <0.05. [d] nd, not detected.

SCHEME 1. Hydroxyl Radical Pathways to Chlorinated Acetic Acids from TCA, PCE, and TCE[a]

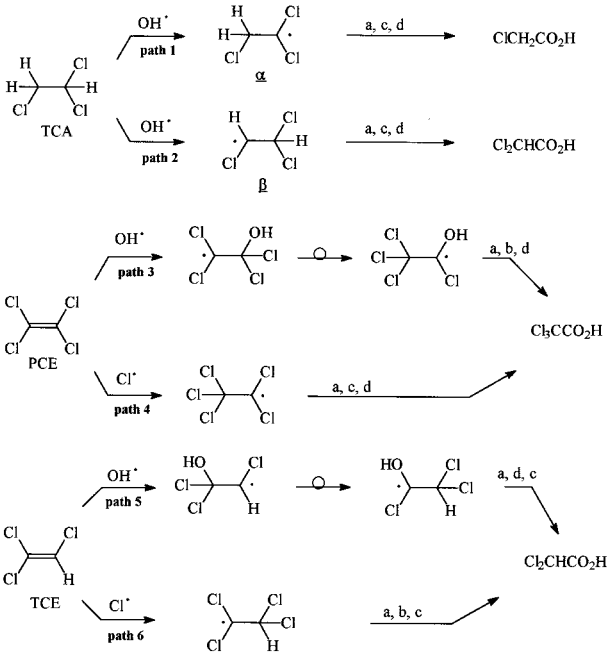

[a] Key: a, reaction with dioxygen to give the peroxyl radical, ROO•; b, dimerization of ROO• to ROOOOR followed by decay of the tetroxide to give an acyl chloride + O_2 + 2Cl• (*41*); c, hydrolysis of the acyl chloride to the carboxylic acid; d, elimination of HO_2• to form an acyl chloride.

Product Distributions of Chlorinated Hydrocarbons. Table 2 lists the chlorinated organic products and their yields for TCA, PCE, and TCE reaction by photo-Fenton as compared to H_2O_2/UV. These products include mono-, di-, and trichloroacetic acids and dichloroacetaldehyde. Non-chlorinated products were not determined. The yields of a given chlorinated product are often similar—within a factor of 2−3—for the two reactions. In several cases, however, there are major differences. Compared to H_2O_2/UV, the photo-Fenton reaction produces ~10 times more dichloroacetic acid from TCA, ~30 times more trichloroacetic acid from PCE, and ~20 times more dichloroacetic acid from TCE. These results could be due either to an effect of iron on reactions occurring after OH•—initiated reactions or by reaction with alternative oxidant(s). We believe the latter is more likely.

Scheme 1 shows the reaction pathways of OH• with TCA, PCE, and TCE leading to chlorinated acids based on radiolysis studies in aerated water (*43*−*45*). The chlorinated products are formed in minor yield alongside mineral products and non-chlorinated organic products. Characteristically, unless a Cl-atom shift occurs, the carbon bearing the unpaired electron after initial OH• attack is functionalized to a carboxylic acid group via a series of irreversible reactions (indicated in Scheme 1) beginning with dioxygen adduct formation.

Hydroxyl reacts with TCA to form mono- and dichloroacetic acids (paths 1 and 2) (*43*, *44*). The initial step is H-abstraction. Monochloroacetic acid (path 1) is favored due to preferential attack of OH• on the H of the Cl_2 carbon for electronic reasons. This is consistent with the mono/di ratio of ~100 obtained under H_2O_2/UV conditions (Table 2). The photo-Fenton reaction, however, gives a much higher yield of dichloroacetic acid at the expense of monochloroacetic acid (mono/di ratio, ~3). Iron(II) and iron(III) ions cannot affect the course of initial OH• attack unless they are somehow coordinated to the OH•. Iron ions are also not expected to affect product distribution in subsequent steps: reduction of the organoradical α or β by Fe(II) merely regenerates starting compound; Fe(III) oxidation of α or β leads, after hydration, simply to the *same* carboxylic acid as dioxygenation. On the other hand, the enhanced yield of dichloroacetic acid can be explained on the basis of an iron-containing oxidant, such as a ferryl, if we presume the bulky iron complex for steric reasons would have a greater tendency than OH• to attack the less-hindered, but electronically *dis*favored position (eq 21).

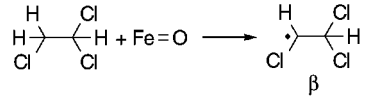

(21)

The reaction of PCE with radiolysis-produced OH• gives low yields of trichloro- and dichloroacetic acids (*44*, *45*). The trichloro-/dichloroacetic acid ratio in the H_2O_2/UV reaction is 0.6, while the same ratio in the photo-Fenton reaction is 18.5 (Table 2). The key step (Scheme 1) in trichloroacetic acid formation is proposed to be either (path 3) 1,2-Cl shift within the PCE-OH• adduct (*44*) or (path 4) addition of Cl• (produced in secondary reactions) to the double bond (*41*, *46*). Reaction of OH• with TCE gives 0.12% dichloroacetic acid and a trace of trichloroacetic acid, while the photo-Fenton reaction gives 2.7% dichloroacetic acid and a trace of trichloroacetic acid (Table 2). The TCE pathway to dichloroacetic acid is not known, but by analogy to PCE, two routes are plausible (refer to Scheme 1): (path 5) addition of OH• to the less-favored carbon, followed by 1,2-Cl shift and (path 6) addition of Cl• to the double bond.

Again, iron cannot influence OH• attack on PCE or TCE unless it coordinates with OH•. Nor can iron influence Cl atom shifts except through coordination, which is unreasonable. The involvement of iron in subsequent steps merits consideration. First, for TCE, one may envision a role of Fe(II) in the enhanced yield of dichloroacetic acid through the pathway in eq 22 in which OH• adds to the (favored) less-substituted carbon, followed by hydrolysis, reduction by Fe(II) to dichloroacetaldehyde, and oxidation to the corresponding carboxylic acid. However, dichloroacetaldehyde was not found, despite being readily detectable in the TCA reaction.

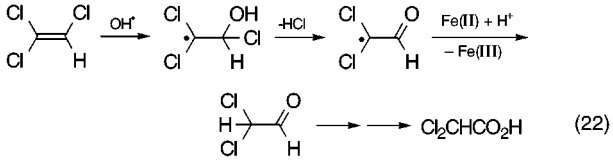

(22)

Second, it is possible that iron ions could increase free Cl• concentrations via ligand-to-metal charge-transfer photolysis ($FeCl^{2+} + h\nu \rightarrow Fe^{2+} + Cl^{\bullet}$) (*47*), especially later in the reaction

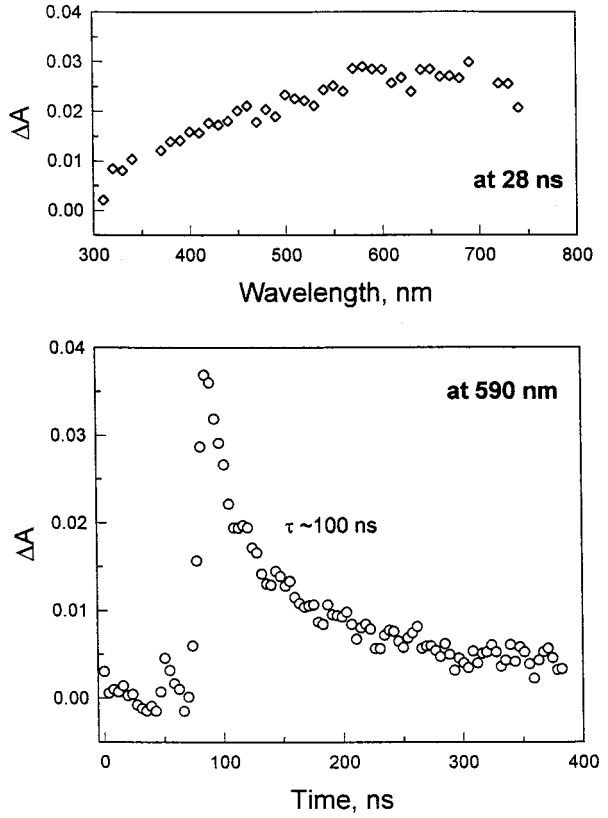

FIGURE 5. Net absorption at 28 ns and kinetic profile of transient absorption at 590 nm after 355 nm laser pulse (pulse length = 6 ns) excitation of aqueous solution containing 1 mM Fe^{3+} and 2 M H_2O_2 at pH 2.80.

as Cl^- becomes more available. This, in turn, could boost the yields of trichloroacetic acid from PCE and dichloroacetic acid from TCE via paths 4 and 6. But the prospect of this reaction is greatly diminished by the low formation constant for $FeCl^{2+}$ ($K = \sim 1$; hence, $[FeCl^{2+}] = \sim 10^{-8}$ M) and the relatively small quantum efficiency (0.13; *47*).

With the caveat that iron does not participate in reactions along the $OH^\bullet$ pathways to alter product distributions of PCE and TCE, we suggest that the enhanced yields of trichloroacetic acid from PCE and of dichloroacetic acid from TCE in the photo-Fenton reaction are due to epoxidation of the parent alkene by ferryl, which is typical for this species:

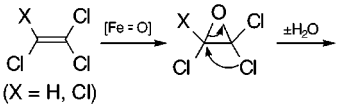

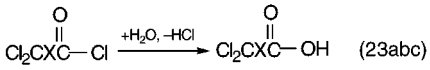

(23abc)

The epoxides of PCE and TCE hydrolyze rapidly in water (eq 23b; $k_{PCE}^{hydrol} = 0.06\ min^{-1}$; $k_{TCE}^{hydrol} = 0.53\ min^{-1}$) *accompanied by Cl migration* to give trichloroacetic acid and dichloroacetic acid, respectively (eq 23bc) (*48*). This could account for their enhanced yields in the photo-Fenton reaction as compared to the H_2O_2/UV reaction.

Fast Kinetics Spectroscopy. Nanosecond laser flash photolysis using a 355-nm laser pulse was used to detect light-induced transient formation in the photo-Fenton reaction in the absence of organic substrate. A broad positive signal in the visible region appeared in solutions containing Fe^{III} and H_2O_2 (Figure 5). This signal is the sum of absorbance by transient(s) and bleaching due to disappearance of precursor molecules. The signal was absent in solutions containing Fe^{III} alone or H_2O_2 alone. The signal at 590 nm exhibits an exponential decay with a lifetime (τ) of about 100 ns (Figure 5). The optical properties of this transient rule out $OH^\bullet$ (*49*) and $HO_2^\bullet$ (*50*), which do not absorb above 350 nm, as well as e^-_{aq}, which has a much smaller τ (<1 ns) under these conditions. Its identity is discussed in the next section.

Remarks on Identity, Origin, and Significance of the Additional Oxidant. Taken as a whole, the evidence is convincing that an additional oxidant is present in photo-Fenton reactions under the present experimental conditions. This oxidant must contain the element of iron. A ferric peroxo complex that could be the precursor has been identified and is formed in significant quantities at iron and hydrogen peroxide concentrations relevant to waste treatment applications.

The identity of the oxidant is undetermined by this study, but its behavior is ferryl-like (Fe^{IV}=O or Fe^{V}=O), including a cyclohexane KDIE consistent with expectation and the ability to catalyze epoxidation. The larger KDIE of the oxidant (1.4) as compared to $OH^\bullet$ (1.1) denotes a transition state for H-abstraction or O-insertion further along the reaction coordinate and, therefore, a species of slightly lower reactivity and greater selectivity. The KDIE for abstraction of OH(D) of 4-fluorophenol by tetra(2-*N*-methylpyridyl)porphyrin oxoiron(IV) (T2MPyP—Fe^{IV}=O) in buffered aqueous solution is 1.32 (*51*). The KDIEs for alkane hydroxylation by porphyrin ferryl complexes range from 2 to 22 according to Sorokin et al. (*52*). They proposed that the KDIE depends strongly on the Fe···O···HR angle in the transition state, a bent geometry giving values around 2.

The broad visible absorption of the transient observed by laser flash photolysis is in accord with the literature on high-valent oxoiron species containing only aquo ligands. The absorbance of $H_3Fe^{V}O_4$ (*26*) and FeO^{3+} (*28*) mentioned in the Introduction extend well into the visible region. The reported absorbance of FeO^{2+} (*27*) extends to at least 340 nm, the limit of those authors' calculations. The short lifetime of the transient (~100 ns) may be a consequence of its reaction with H_2O_2, which was present at 2 M in this experiment. [In the absence of oxidizable organic compounds, FeO^{2+} decomposes rapidly to Fe^{III} by reaction with H_2O_2 or itself (*26*, *27*).] Alternatively, the spectrum of the transient may represent the triplet excited state of $[Fe^{III}—OOH]^{2+*}$ (eq 24).

The photochemistry of Fe^{III} is dominated by ligand-to-metal charge transfer (LMCT) processes in which the iron is reduced (*18*). For this case, eq 25, the product is the unreactive $HO_2^\bullet$ radical however. Equation 25 was proposed on the basis of O_2 quantum yields (*54*).

$$[Fe^{III}—OOH]^{2+} \overset{h\nu}{\rightleftharpoons} [Fe^{III}—OOH]^{2+*} \quad (24)$$

$$[Fe^{III}—OOH]^{2+*} \rightarrow Fe^{II} + HO_2^\bullet \quad (25)$$

$$[Fe^{III}—OOH]^{2+*} \rightarrow \{Fe^{III}—O^\bullet \leftrightarrow Fe^{IV}=O\} + {}^\bullet OH \quad (26)$$

$$[Fe^{III}—OOH]^{2+*} \rightarrow Fe^{V}=O + OH^- \quad (27)$$

Reaction 26 produces ferryl where iron is formally in the +IV oxidation state. The structure is really a hybrid in which unpaired electron density exists on O. Reaction 26 may be regarded as either a metal-to-ligand charge transfer (MLCT) reaction—which is rare or unknown for Fe^{III} (*18*)—or an intraligand (IL) reaction analogous to H_2O_2 photolysis, which is efficient throughout the UV (eq 5; $\phi_{OH} = 1$, 195–350 nm). Ab initio calculations (*17*) show that photolysis of H_2O_2 above 170 nm occurs by excitation of an electron from a lone pair highest occupied molecular orbital (HOMO) having π-antibonding character with respect to the O—O linkage, to a lowest unoccupied molecular orbital (LUMO) having σ^*

character. In Fe^{III}−OOH, the HOMO (π-antibonding with respect to O−O) has the proper symmetry for overlap with a metal *d* orbital. This overlap can assist IL O−O bond cleavage by providing a conduit for an electron to "leave" the metal and stablize the nascent oxo radical ligand. A related reaction is the proposed photolysis of binuclear iron complexes to give iron(IV) ferryl (*18*, *53*): $L-Fe^{III}-O-Fe^{III}-L \rightarrow \{L-Fe^{III}-O^{\bullet} \leftrightarrow Fe^{IV}=O\} + Fe^{II}-L$ (e.g., L = EDTA). That reaction is said to involve metal-to-metal charge transfer. Reaction 27 represents a heterolytic O−O bond cleavage to give iron(V) ferryl and hydroxide ion. As a primary photochemical step, it should be regarded as highly unlikely since it involves an unprecedented two-electron metal-to-ligand charge transfer. In summary, a photochemical origin of the putative ferryl is possible, but the options are not entirely satisfactory. Thus, we cannot rule out the possibility that ferryl is formed in secondary thermal reactions (*28*, *29*).

The contribution of the additional oxidant we have detected to the rates of oxidation of organic compounds in photo-Fenton treatment applications will require further research. The presumed precursor, $[FeO_2H]^{2+}$, absorbs further out into the visible region than Fe^{III}_{aq}, capturing more of the light there. This study suggests that, at a minimum, the new oxidant may have a significant affect on product distributions. Ferryl likely plays a minor, if any, role in the chemistry of natural waters because Fe^{III}_{aq} and H_2O_2 concentrations are ordinarily too small to form the presumed precursor complex in significant yields.

Acknowledgments

We thank Drs. Prashant Kamat and Richard Fessenden at the DOE Radiation Laboratory, University of Notre Dame, for their assistance with the laser experiments and Janet Sanford for technical assistance. Funding was provided by the National Science Foundation (BES-9414594).

Literature Cited

(1) Meunier, B. In *Metalloporphyrins Catalyzed Oxidations*; Montanari, F., Casella, L., Eds.; Kluwer Academic Publishers: Dordrecht, 1994; Chapter 1.
(2) Feig, A. L.; Lippard, S. J. *Chem. Rev.* **1994**, *94*, 759−805.
(3) Fujii, H.; Yoshimura, T.; Kamada, H. *Inorg. Chem.* **1996**, *35*, 2373−2377.
(4) Sawyer, D. T.; Sobkowiak, A.; Matsushita, T. *Acc. Chem. Res.* **1996**, *29*, 409−416.
(5) Moffett, J. W.; Zika, R. G. *Environ. Sci. Technol.* **1987**, *21*, 804−810.
(6) Faust, B. C. *Environ. Sci. Technol.* **1994**, *28*, 217A−222A.
(7) Pignatello, J. J. *Environ. Sci. Technol.* **1992**, *26*, 944−951.
(8) Sun, Y.; Pignatello, J. J. *Environ. Sci. Technol.* **1993**, *27*, 304−310.
(9) Chen, R.; Pignatello, J. J. *Environ. Sci. Technol.* **1997**, *31*, 2399−2406.
(10) Bauer, R.; Fallmann, H. *Res. Chem. Intermed.* **1997**, *23*, 341−354.
(11) Safarzadeh-Amiri, A.; Bolton, J. R.; Cater, S. R. *Sol. Energy* **1996**, *5*, 439−443.
(12) Watts, R.; Kong, S.; Dippre, M.; Barnes, W. T. *J. Hazard. Mater.* **1994**, *39*, 33−47.
(13) Aronstein, B. N.; Lawal, R. A. L.; Maka, A. *Environ. Toxicol. Chem.* **1994**, *13*, 1719−1726.
(14) Pignatello, J. J.; Day, M. *Hazard. Waste Hazard. Mater.* **1996**, *13*, 237−244.
(15) Barb, W. G.; Baxendale, J. H.; George, P.; Hargrave, K. R. *Trans. Faraday Soc.* **1951**, *47*, 591−616.
(16) Walling, C. *Acc. Chem. Res.***1975**, *8*, 125−131.
(17) Chevaldonnet, C.; Cardy, H.; Dargelos, A. *Chem. Phys.* **1986**, *102*, 55−61.
(18) Horváth, O.; Stevenson, K. L. *Charge-Transfer Photochemistry of Coordination Compounds*; VCH Publishers: New York, 1993.
(19) Conocchioli, T. J.; Hamilton, E. J., Jr.; Sutin, N. *J. Am. Chem. Soc.* **1965**, *87*, 926−927.
(20) Kremer, M. L. *Int. J. Chem. Kinet.* **1985**, *17*, 1299−1314.
(21) Wink, D. A.; Nims, R. W.; Desresiers, M. F.; Ford, P. C.; Keefer, L. K. *Chem. Rev. Toxicol.* **1991**, *4*, 510−512.
(22) Walling, C.; Amarnath, K. *J. Am. Chem. Soc.* **1982**, *104*, 1185−1189.
(23) Dong, Y.; Fujii, H.; Hendrich, M. P.; Leising, R. A.; Pan, G.; Randall, C. R.; Wilkinson, E. C.; Zang, Y.; Que, L., Jr.; Fox, B. G.; Kauffmann, K.; Munck, E. *J. Am. Chem. Soc.* **1995**, *117*, 2778−2792.
(24) Arasasingham, R. A.; Cornman, C. R.; Balch A. L. *J. Am. Chem. Soc.* **1989**, *111*, 7800−7805.
(25) Rahhal, S.; Richter, H. W. *J. Am. Chem. Soc.* **1988**, *110*, 3126−3133.
(26) Rush, J. D.; Bielski, B. H. J. *Inorg. Chem.* **1994**, *33*, 5499−5502.
(27) Løgager, T.; Holcman, J.; Sehested, K.; Pedersen, T. *Inorg. Chem.* **1994**, *33*, 3523−3529.
(28) Kremer, M. L.; Stein, G. *Trans. Faraday Soc.* **1959**, *55*, 959−973.
(29) Bossmann, S. H.; Oliveros, E.; Göb, S.; Siegwart, S.; Dahlen, E. P.; Payawan, L., Jr.; Straub, M.; Worner, M.; Braun, A. M. *J. Phys. Chem.* **1998**, *102*, 5542−5550.
(30) Zepp, R. G.; Faust, B. C.; Hoigné, J. *Environ. Sci. Technol.* **1992**, *26*, 313−319.
(31) Haag, W. R.; Yao, C. C. D. *Environ. Sci. Technol.* **1992**, *26*, 1005−1013.
(32) Jiang, J.; Bank, J. F.; Scholes, C. *J. Am. Chem. Soc.* **1993**, *115*, 4742−4746.
(33) Knight, R. J.; Silva, R. N. *J. Inorg. Nucl. Chem.* **1975**, *37*, 779−783.
(34) Knapp, D. R. *Handbook of Analytical Derivatization*; John Wiley & Sons: New York, 1979; Chapter 3, pp 146−224.
(35) Millburn, R. M.; Vosburgh, W. C. *J. Am. Chem. Soc.* **1955**, *77*, 1352−1355.
(36) Lewis, T. J.; Richards, D. H.; Salter, D. A. *J. Chem. Soc.* **1963**, 2434−2446.
(37) Evans, M. G.; George, P.; Uri, N. *Trans. Faraday Soc.* **1949**, *34*, 230−239.
(38) Buxton, G. V.; Greenstock, C. L.; Helman, W. P.; Ross, A. B. *J. Phys. Chem. Ref. Data* **1988**, *17*, 513−886.
(39) Lee, K. A.; Nam, W. *J. Am. Chem. Soc.* **1997**, *119*, 1916−1922.
(40) Onuoha, A. C.; Zu, X. L.; Rusling, J. F. *J. Am. Chem. Soc.* **1997**, *119*, 3979−3986.
(41) von Sonntag, C.; Schuchmann, H.-P. In *Peroxyl Radicals*; Alfassi, Z. B., Ed.; John Wiley & Sons: Chichester, U.K., 1997; Chapter 8, pp 173−234.
(42) Punniyamurthy, T.; Bhatia, B.; Iqbal, J. *J. Org. Chem.* **1994**, *59*, 850−853.
(43) Lal, M.; Monig, J.; Asmus, K.-D. *J. Chem. Soc., Perkin Trans. 2* **1987**, 1639−1644.
(44) Mao, Y.; Schöenich, C.; Asmus, K.-D. *J. Phys. Chem.* **1991**, *95*, 10080−10089.
(45) Mao, Y.; Schöenich, C.; Asmus, K.-D. In *Photoctalytic Purification and Treatment of Water and Air*; Ollis, D. F., Al-Ekabi, H., Eds.; Elsevier: New York, 1993; pp 49−66.
(46) Mertens, R.; von Sonntag, C. *J. Chem. Soc., Perkin Trans. 2* **1994**, 2181−2185.
(47) Balzani, V.; Carassiti, V. *Photochemistry of Coordination Compounds*; Academic Press: New York, 1970; Chapter 10, pp 145−192.
(48) Kline, S. A.; Solomon, J. J.; Van Duuren, B. L. *J. Org. Chem.* **1978**, *43*, 3596−3600.
(49) Nielsen, S. O.; Michael, B. D.; Hart, E. J. *J. Phys. Chem.* **1976**, *80*, 2482−2488.
(50) Bielski, B. H. J. *Photochem. Photobiol.* **1978**, *28*, 645−649.
(51) Colclough, N.; Lindsay Smith, J. R. *J. Chem. Soc., Perkin Trans. 2* **1994**, 1139−1149.
(52) Sorokin, A.; Robert, A.; Meunier, B. *J. Am. Chem. Soc.* **1993**, *115*, 7293−7299.
(53) Kunkely, H.; Vogler, A. *J. Chem. Soc. Chem. Commun.* **1994**, 2671−2672.
(54) Behar, B.; Stein, G. *Science* **1986**, *154*, 1012−1013.

Received for review September 21, 1998. Revised manuscript received February 12, 1999. Accepted March 10, 1999.

ES980969B